

TWO RADIO-EMISSION MECHANISMS IN PSR J0901–4624

C. A. RAITHEL^{1,2}, R. M. SHANNON^{1,3}, S. JOHNSTON¹, & M. KERR¹¹ CSIRO Astronomy and Space Science, Australia Telescope National Facility, Box 76 Epping, NSW 1710, Australia, and² Department of Physics and Astronomy, Carleton College, Northfield, MN 55057 USA*Draft version October 26, 2018*

ABSTRACT

We have detected sporadic, bright, short-duration radio pulses from PSR J0901–4624. These pulses are emitted simultaneously with persistent, periodic emission that dominates the flux density when averaging over many periods of the pulsar. The bright pulses have energies that are consistent with a power-law distribution. The integrated profile of PSR J0901–4624 is highly polarized and shows four distinct components. The bright pulses appear to originate near the magnetic pole of the pulsar and have polarization properties unlike that of the underlying emission at the same pulse phase. We conclude that the bright pulses represent a secondary giant-micropulse emission process, possibly from a different region in the pulsar magnetosphere.

Subject headings: pulsars: general — pulsars:individual (PSR J0901–4624) — stars:neutron

1. INTRODUCTION

Since the discovery of pulsars, the phenomenology associated with their radio emission has been a fertile source for studying coherent-emission processes in magnetized plasma. It is clear that although the time-integrated profiles of radio pulsars are constant or nearly constant, individual pulses that go into creating the integrated profile are highly variable both in total intensity and in their polarization.

Historically, there has been an understanding that the fluence of individual pulses follows either a log-normal or Gaussian distribution (Cairns, Johnston & Das 2001, 2003; Burke-Spolaor et al. 2012; Shannon et al. 2014) with relatively few pulses significantly stronger than the mean. We will refer to this distribution as the normal-mode of emission. The main exception to this has been the giant pulses observed from the Crab pulsar (Staelin & Reifenstein 1968), which are extremely bright ($\gtrsim 1$ MJy) and narrow ($\ll 10$ ns) bursts emitted at certain pulse phases (Hankins et al. 2003).

More recently, a sub-set of pulsars have been identified that show highly erratic behaviour in their single pulses. The giant-pulse mode was seen in other young (Johnston & Romani 2003) and millisecond pulsars (Cognard et al. 1996; Romani & Johnston 2001; Knight et al. 2006). Several young, energetic pulsars show single-pulse variability similar to the giant-pulse mode, except that the bursts have μ s rather than ns widths (Johnston et al. 2001; Johnston & Romani 2002), which has been referred to as the giant-micropulse emission.

Emission from less energetic pulsars and millisecond pulsars also shows phase dependent variability, including power-law statistics on the leading or trailing edges.

One of the best-studied slow pulsars, PSR B1133+16 shows, at high frequencies ($\nu > 4$ GHz) individual pulses with power-law statistics, of ~ 2 ms width (Kramer et al. 2003; Krzeszowski et al. 2014). The bright pulses orig-

inate predominantly from the trailing edge of the first component of the double-cone profile. At low frequencies, the bright pulses originate on both components (Kramer et al. 2003). The brightest pulses from the millisecond pulsar PSR J1713+0747 originate from the trailing edge of the main component (Shannon & Cordes 2012). However these pulses show a lognormal energy distribution. In contrast, the brightest pulses in PSR J0437–4715 originate from the center of the profile. These stronger pulses have fractionally higher polarization than weaker pulses (Osłowski et al. 2014).

Rotating Radio Transients (RRATs, McLaughlin et al. 2006) emit single pulses extremely sporadically, with pulses emitted every few minutes or longer. While some of the pulsars in this group also have underlying normal-mode emission, some do not (Ridley 2010). Further complicating the picture, several pulsars appear to have a combination of normal-mode, and RRAT-like behaviour (Weltevrede et al. 2006; Weltevrede, Johnston & Espinoza 2011).

Here we report the discovery of a new example of sporadic, bright emission from PSR J0901–4624. Bright pulses from J0901–4624 show a power-law distribution, which are weaker and broader than giant pulses but occur more frequently than giant micropulses identified from previous pulsars. In addition, we compare the bright pulses of J0901–4624 to other modes of pulsar emission.

2. OBSERVATIONS

During a monitoring programme of ~ 180 young pulsars at the 64-meter Parkes radio telescope in support of the Fermi Space Telescope mission (Weltevrede et al. 2010), using a real-time transient search algorithm (Barsdell et al. 2012), we identified occasional (once per 20 s) bright ($S/N > 20$), narrow ($< 500 \mu$ s) pulses being emitted from PSR J0901–4624. With a rotation period of 442 ms, a dispersion measure of 199 pc cm^{-3} , and an inferred spin-down energy of $4.0 \times 10^{34} \text{ erg s}^{-1}$, PSR J0901–4624 has median properties for the sample selected for high spin-down energy.

³ E-mail: ryan.shannon@csiro.au

To examine the bright pulses in more detail, we observed PSR J0901–4624 again with the Parkes telescope on six separate occasions, of 30 – 60 min in duration, as listed in Table 1. All observations were made using the 21-cm multibeam system at a central frequency close to 1400 MHz. The system-equivalent flux density of the system is ~ 35 Jy on cold regions of the sky.

Data were recorded using three backend systems operating in parallel. The first backend (PDFB4) produced a period-averaged digital-filterbank output of 256 MHz bandwidth, centered at 1369 MHz, comprising 1024 frequency channels for each of 1024 phase bins across the pulse period for both the two auto correlations and the real and imaginary parts of the cross correlations of the feed probes. Data were folded at the topocentric pulse period and accumulated for 30 s and recorded to disk. The second system (PDFB3) produced fast-sampled digital-filterbank output with 256 MHz bandwidth centered at 1369 MHz, with 512 frequency channels per polarization sampled every $256 \mu\text{s}$. Finally, on May 25 we used a baseband recording system (CASPSR), with 400 MHz bandwidth centered at 1382 MHz in order to resolve short-duration signals and mitigate intra-channel dispersion smearing in observations with the filterbank-spectrometer systems. The DSPSR software package (van Straten & Bailes 2011) was used to subdivide the data into single rotations of the pulsar for the PDFB3 and CASPSR datasets. In the case of CASPSR, DSPSR was also used to coherently disperse the data.

A calibration signal, injected into the feed at an angle of 45° with respect to the probes, was recorded before each observation. This signal was used to determine the relative gain and phase of the two polarization probes.

Data editing and calibration were conducted using the PSRCHIVE package (Hotan, van Straten & Manchester 2004). In brief, after removal of radio-frequency interference in both the frequency and time domains, the data were gain and polarization calibrated and summed in frequency and time to produce a pulse profile for each pulsar observed. Data were flux calibrated using observations of the radio galaxy Hydra A made as part of the Parkes Pulsar Timing Array project (Manchester et al. 2013). Details of the observations can be found in Table 1.

3. INTEGRATED PROFILE

In the top panel of Fig 1, we show the full-Stokes profile and linear polarization position angle for PSR J0901–4624, formed from co-adding all of our observations. The profile consists of four distinct components with a total width of 27° . The geometric center of the profile occurs between the two inner components, which indicates the pulsar has double-conal structure. The pulsar is highly linearly polarized, which is typical for young, high- \dot{E} pulsars. PSR J0901–4624 also shows a high degree of circular polarization in the trailing component (Johnston & Weisberg 2006; Weltevrede & Johnston 2008); it is common for the trailing component to have the dominant amplitude and significant circular polarization (Johnston & Weisberg 2006).

The position-angle swing is well described by the rotating-vector model with the best-fitting model giving an inflexion point located 3.9° after the geometric cen-

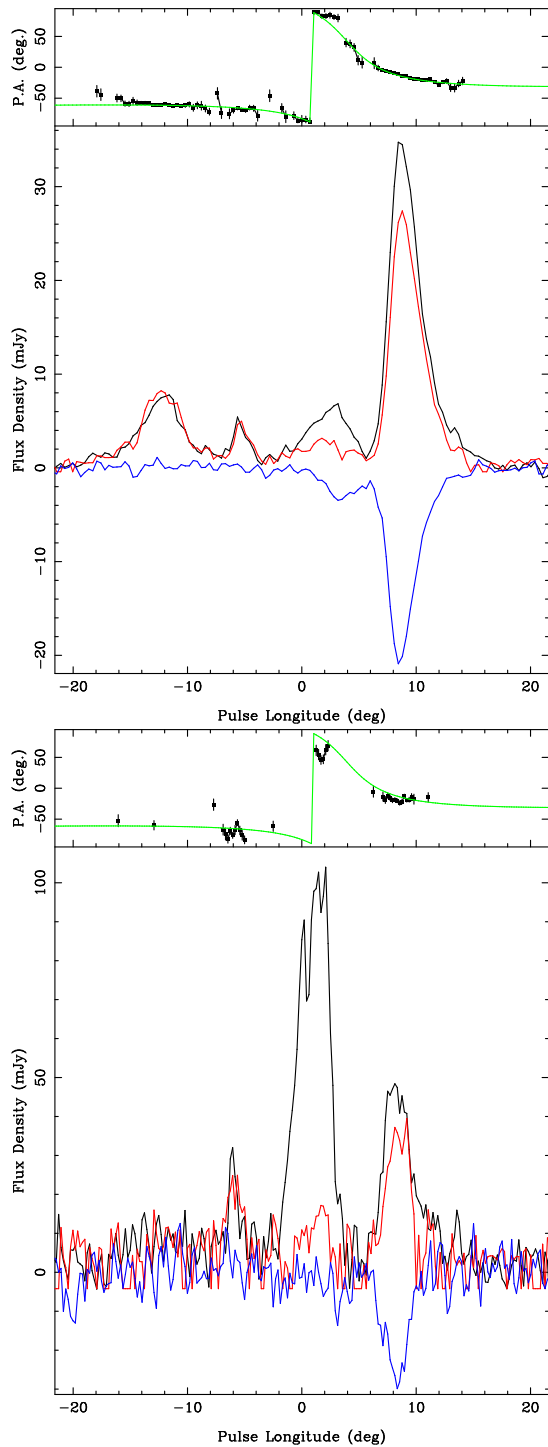


FIG. 1.— Upper panel: Integrated profile of PSR J0901–4624 in full Stokes at 1369 MHz. The lower plot shows the total intensity (black line), linear polarization (red line) and circular polarization (blue line) as a function of pulse longitude. The top panel shows the position angle of the linearly polarized radiation and runs between -90° and $+90^\circ$. The green line is the best-fitting model of the beam geometry to the position-angle data. Phase zero is chosen to be the geometric center of the profile. The dominant features in the profile are four components centered at longitudes of -12° , -6° , 4° , and 9° relative to the geometric center. Lower panel: Profile formed from only the bright ($S/N > 5$) pulses. Bright pulses originate primarily from the central component and have a width of 1-2 bins of phase resolution. The RVM model is the same as in the upper panel.

TABLE 1
OBSERVATION DETAILS

Date (MJD)	N	N_5	\bar{S}_ν (mJy)
May 17	8148	32	0.66
May 25	8156	33	0.69
July 25	7034	72	0.95
July 27	2197	17	0.85
Aug 19	4085	13	0.63
Sep 28	4085	5	0.51

NOTE. — For each epoch, we list the N , number of rotations of the pulsar observed; N_5 , the number of $5 - \sigma$ pulses detected, and \bar{S}_ν , the mean observed flux density.

ter of the profile. This can be used to infer an emission height of ~ 700 km, or about 3% of the light-cylinder radius. Using the method of Rookyard et al. (2014) we determine a best-fitting value for the inclination of the rotation axis to the magnetic axis of $\alpha \sim 50^\circ$ and an impact parameter of $\beta \sim 2^\circ$.

Observations of the pulsar have also been made at 3.1 GHz and 0.7 GHz. There is little evolution of the profile over this frequency range.

4. INDIVIDUAL PULSES

In total, over the six observations we observed $\sim 34,000$ rotations of the pulsar. Approximately ~ 400 pulses with a $S/N > 5$ were identified. All of these bright pulses had narrow width (< 1 ms). The daily variation in the rate of bright pulses, as shown in Table 1 is caused by scintillation and the distribution of pulse energies (see section 5). After accounting for these effects, consistent numbers of bright pulses were detected on each day.

Based on observations made with the CASPSR coherent dedispersion system, the full-width half maximum of the bright pulses varies between $130 \mu\text{s}$ and $400 \mu\text{s}$, which is less than 0.1% of the pulse period. Two of the brightest pulses from these observations are displayed in Figure 2. The location of the bright pulses varies in location by approximately 4° in pulse phase (1% of the period). Occasionally bright pulses are seen from the two components that flank the central component. The time between bright pulses is consistent with a Poisson random process.

In the lower panel of Figure 1, we show the average profile formed by combining only the brightest pulses. These pulses greatly enhance the emission at the center of the integrated profile. We note that the rarity of bright pulses results in very little overall effect on the integrated profile. In addition, we see the bright pulses are emitted simultaneously with the underlying, fainter emission. The normal emission observed during the bright pulses ($S_{\text{peak,bright}} \sim 50$ mJy) is modestly brighter during all of the pulses ($S_{\text{peak,all}} \sim 35$ mJy) suggesting that there may be a connection between the two modes of emission.

4.1. Polarization Properties

The integrated profile of PSR J0901–4624 is highly linearly polarized (top panel of Figure 1). This implies that one orthogonal mode dominates the emission

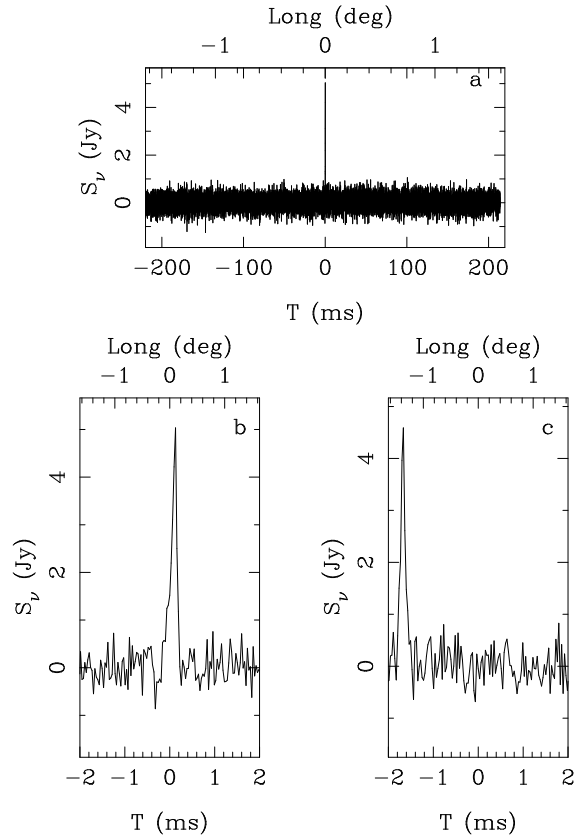


FIG. 2.— Two bright pulses taken from our coherently dedispersed observations with CASPSR. The data have been binned to provide $32 \mu\text{s}$ resolution. Panel *a* Full rotation of PSR J0901–4624. Panels *b* and *c* zoom-in of pulse displayed in Panel *a*. Panel *c*: Second bright pulse.

(Johnston et al. 2005) and that the single pulses should also be highly polarized. For the normal emission this is indeed the case. We occasionally detect bright pulses from component 2 and 4 which are highly polarized (see lower panel of Figure 1).

In contrast, the bright emission has very different polarization as can be seen in Figure 1. In the centre of the profile, where the bright emission originates, almost no polarization is seen and what little polarization there is has a different polarization-angle swing to that of the normal emission. This is unusual behaviour and hints at a different origin for the normal and bright emissions.

5. FLUX DISTRIBUTION

We analyzed the flux distribution using the single-pulse PDFB4 data. We identified bright pulses by first identifying the brightest bin in a window of 14° width in pulse phase centered on the third component of the average profile. We then calculated three signal-to-noise (S/N) ratios using an estimate of the off pulse noise: the first from only the brightest bin, and the second and third from the sum of the brightest and its two adjacent bins. We only searched for narrow pulses after a first inspection of the data revealed that the bright pulses were either unresolved (< 1 bin of pulse phase for the lower time resolution PDFB4 data) or marginally resolved. Of these three, we report the integrated pulse energy with the largest S/N . To assess the expected distribution of

noise, we repeated the same algorithm using a control sample of the same width in a region of pulse phase in which no pulsar emission occurs. In Figure 3, we show that the histograms of pulse energy in both the bright pulse window and the off-pulse window.

Because of the relatively low signal-to-noise ratio, it is necessary to deconvolve the noise distribution when modelling the pulse-energy distribution. We used techniques described in Shannon et al. (2014) to deconvolve the noise and model the pulse-energy distribution. The measured pulse energy ρ_E is the convolution of the noise ρ_N and the intrinsic energy ρ_I :

$$\rho_E(E) = \int dE' \rho_N(E') \rho_I(E - E'). \quad (1)$$

The noise distribution ρ_N is non-trivial to calculate because the algorithm used to identify significant pulses results in a non-Gaussian statistics, and refractive scintillation modulates the S/N at each epoch. For a single observing epoch, in which we assume that the scintillation does not significantly affect the pulse energy, by the central limit theorem, the off-pulse samples are expected to be Gaussian distributed. The probability of getting at least one measurement greater than some value E in N trial samples is the converse of the probability of having all values less than E

$$P(E > E') = \frac{1}{2} \left[1 + \operatorname{erf} \left(\frac{E}{\sqrt{2}\sigma} \right) \right]^N. \quad (2)$$

The probability density is the derivative of Equation (2):

$$\rho_N(E) = \frac{N}{2} \left[1 + \operatorname{erf} \left(\frac{E}{\sqrt{2}\sigma} \right) \right]^{N-1} \exp \left[-\frac{x^2}{2\sigma^2} \right]. \quad (3)$$

Because we have averaged together multiple days, after correcting for pulse flux variations caused by scintillation, the noise distribution deviates from theoretical expectation. We therefore fitted an analytic function to the off-pulse noise distribution, shown as the thin, solid line in Figure 3, with N and σ allowed to be free parameters, and we then deconvolved the pulse-energy distribution using this function.

For the pulse energy distribution we considered both log-normal distribution (see Equation 7 of Shannon et al. (2014)) and power-law distribution

$$\begin{aligned} \rho_I(E) &= AE^{-\beta} \exp(-E_c/E) & (E < E_c) \\ &= AE^{-\beta} & (E > E_c), \end{aligned} \quad (4)$$

where β is the spectral index, E_c is a low-energy exponential cutoff, and A is a normalising factor.

We find that models with power-law distributions produced better agreement than models with log-normal distributions. In particular the best-fitting log-normal models do not reproduce the observed high-energy tail. For the best-fitting power-law model, the energy cut-off is $E_c \approx 0.1$ mJy ms and the spectral index is $\alpha = 2.28(4)$. The spectral index is comparable to those measured in other power-law emitting pulsars (Knight et al. 2006).

6. DISCUSSION

One of the major open questions in pulsar emission is how timescales are set for pulse emission. Giant pulses

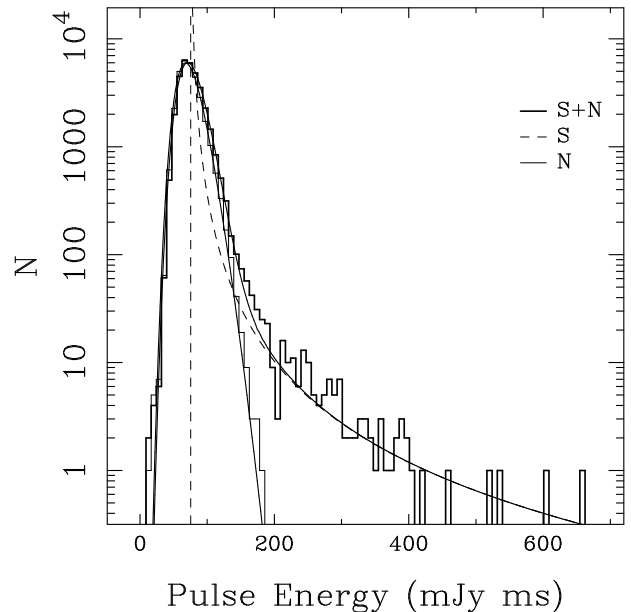


FIG. 3.— Pulse-energy distribution for PSR J0901–4624. The thin solid line labelled N shows a model for the noise. The thin-dashed line labelled S shows the best-fitting power-law model for the pulse energy distribution. The thick solid line (labelled $S + N$) shows the convolved pulse-energy distribution.

have timescale of ns, whereas the intermittent pulsars (Kramer et al. 2006) can remain in quiescent states for years between active states. In between these two extremes are microstructure, single pulse drifting, nulling, mode-changing and RRAT emission. There is clearly a continuum of temporal regimes, but it is important to assess how these variations relate to other pulsar properties such as ages, viewing and beaming geometries, and magnetic field strengths. PSR J0901–4624 shows a secondary emission mode in which bright narrow pulses are frequently emitted from the central component.

Another important differentiator between emission processes is the distribution of the energies of individual pulses (see Cairns, Johnston & Das 2001, and references within). Normal-mode emission (from slow or millisecond pulsars) is observed to have either log-normal or gaussian energy distributions (Burke-Spolaor et al. 2012; Shannon et al. 2014). The situation with RRAT-mode emission is much less clear. The best-studied object with RRAT emission, PSR J1819–1458 shows sporadic pulses that are very similar to normal-mode emission (Karastergiou et al. 2009). However, other RRATs appear to have power-law emission (Ridley 2010). In contrast, giant pulses, giant micropulses of Vela, the trailing bright pulses in PSR B1706–44, and the emission of PSR J0901–4624 follow power-law distributions.

The width of the bright pulses in PSR J0901–4624 seem to lie between the giant pulses (with widths less than 10^{-5} P) and those of the RRATs (with widths greater than 10^{-3} P). The jitter in the arrival times is also greater than in total pulse phase giant-pulse emission, less than RRAT-mode emission, and similar to giant micropulse emission. The widths of the pulses can be connected to the physical scales of the emission region,

with shorter duration pulses implying physically smaller emission regions.

The location of the bright emission also can be used to distinguish emission modes. Giant-pulse emission is associated with gamma-ray emission and likely arises from the outer magnetosphere (Abdo et al. 2010). In contrast, the bright pulses observed from Vela, PSRs B1706–44, B1046–58, B1133+16, and J1713+0747 are not associated with higher energy emission but arise at the edges of the normal-mode emission. Like PSR J0901–4624, the bright pulses from PSR J0437–4715 arise from close to the center of the profile; however these pulses show higher polarization than weaker pulses.

In at least some of the RRATs, emission appears to come from conventional core-cone emission morphology across the whole polar cap (Karastergiou et al. 2009; Keane et al. 2011). In PSR J0901–4624, the bright pulsars seem to originate close to the center of the profile and hence the magnetic pole. There is no detected high-energy emission for PSR J0901–4624, so we do not know if its bright pulses are coincident with a high-energy emitting region.

Finally, the polarization properties of these emission modes are different. Both giant-pulse emission in the Crab (Hankins et al. 2003) and giant micropulse emission in the Vela pulsar (Kramer, Johnston & van Straten 2002) are highly polarised. For the RRAT PSR J1819–1458, the polarization properties are similar to that seen in single pulse emission; the degree of linear polarization varies and orthogonal mode jumps are present (Karastergiou et al. 2009). The bright pulses from PSR J0901–4624 show low levels of polarization, in contrast to its normal-mode emission, which at the same longitude shows a high level of linear polarization.

There are two plausible interpretations for the different emission modes. The bright pulses could arise from a different plasma state or from a different region in the magnetosphere.

Because the bright pulses originate close to the geometric center of the pulse profile, they likely originate from low altitude, and is therefore unlikely to be depolarised by caustic effects. Therefore the low level of polarisation suggests that the emission arises from a different plasma state, for example when the polar gap is plasma-starved. The second state would have to produce normal-mode emission which is observed simultaneously to the bright pulses.

7. CONCLUSIONS

We have detected bright, narrow pulses from PSR J0901–4624. Similar to giant-micropulse emission observed in 4 other young energetic pulsars, the pulse energies follow a power-law distribution. Unlike other giant-micropulse emitters, the pulses originate from the center of the profile. Unlike the normal-mode emission for the pulsar, the bright pulses show low levels of total polarization. These bright pulses could possibly be produced either when the magnetosphere is in a different state or from a different location in the magnetosphere.

ACKNOWLEDGMENTS

We thank the referee for comments that greatly improved the manuscript. The Parkes radio telescope is part of the Australia Telescope National Facility which is funded by the Commonwealth of Australia for operation as a National Facility managed by CSIRO.

REFERENCES

- Abdo A. A. et al., 2010, *ApJ*, 708, 1254
 Barsdell B. R., Bailes M., Barnes D. G., Fluke C. J., 2012, in *Astronomical Society of the Pacific Conference Series*, Vol. 461, *Astronomical Data Analysis Software and Systems XXI*, Ballester P., Egret D., Lorente N. P. F., eds., p. 37
 Burke-Spolaor S. et al., 2012, *MNRAS*, 423, 1351
 Cairns I. H., Johnston S., Das P., 2001, *ApJ*, 563, L65
 Cairns I. H., Johnston S., Das P., 2003, *MNRAS*, 343, 512
 Cognard I., Shrauner J. A., Taylor J. H., Thorsett S. E., 1996, *ApJ*, 457, 81
 Hankins T. H., Kern J. S., Weatherall J. C., Eilek J. A., 2003, *Nature*, 422
 Hotan A. W., van Straten W., Manchester R. N., 2004, *Proc. Astr. Soc. Aust.*, 21, 302
 Johnston S., Romani R., 2002, *MNRAS*, 332, 109
 Johnston S., Romani R., 2003, *ApJ*, 590, L95
 Johnston S., van Straten W., Kramer M., Bailes M., 2001, *ApJ*, 549, L101
 Johnston, S., Hobbs, G., Vigeland, S., et al. 2005, *MNRAS*, 364, 1397
 Johnston S., Weisberg J. M., 2006, *MNRAS*, 368, 1856
 Karastergiou A., Hotan A. W., van Straten W., McLaughlin M. A., Ord S. M., 2009, *MNRAS*, 396, L95
 Keane E. F., Kramer M., Lyne A. G., Stappers B. W., McLaughlin M. A., 2011, *MNRAS*, 415, 3065
 Knight H. S., Bailes M., Manchester R. N., Ord S. M., Jacoby B. A., 2006, *ApJ*, 640, 941
 Kramer M., Johnston S., van Straten W., 2002, *MNRAS*, 334, 523
 Kramer, M., Karastergiou, A., Gupta, Y., et al. 2003, *A&A*, 407, 655
 Kramer M., Lyne A. G., O’Brien J. T., Jordan C. A., Lorimer D. R., 2006, *Science*, 312, 549
 Krzeszowski, K., Maron, O., Słowikowska, A., Dyks, J., & Jessner, A. 2014, *MNRAS*, 440, 457
 Manchester R. N. et al., 2013, *Proc. Astr. Soc. Aust.*, 30, 17
 McLaughlin M. A. et al., 2006, *Nature*, 439, 817
 Osłowski, S., van Straten, W., Bailes, M., Jameson, A., & Hobbs, G. 2014, *MNRAS*, 441, 3148
 Ridley J. P., 2010, PhD thesis, West Virginia University
 Romani R., Johnston S., 2001, *ApJ*, 557, L93
 Shannon, R. M., & Cordes, J. M. 2012, *ApJ*, 761, 64
 Shannon R. M. et al., 2014, *MNRAS*, 443, 1463
 Staelin D. H., Reifenstein, III E. C., 1968, *Science*, 162, 1481
 van Straten W., Bailes M., 2011, *Proc. Astr. Soc. Aust.*, 28, 1
 Weltevredre P., Johnston S., 2008, *MNRAS*, 391, 1210
 Weltevredre P., Johnston S., Espinoza C. M., 2011, *MNRAS*, 411, 1917
 Weltevredre P. et al., 2010, *Proc. Astr. Soc. Aust.*, 27, 64
 Weltevredre P., Stappers B. W., Rankin J. M., Wright G. A. E., 2006, *ApJ*, 645, L149